LETTERS
https://doi.org/10.1038/s41567-018-0069-0
nature physics

Attosecond optical-field-enhanced carrier injection into the GaAs conduction band

F. Schlaepfer[1*], M. Lucchini[1,3], S. A. Sato[2], M. Volkov[1], L. Kasmi[1], N. Hartmann[1], A. Rubio[2], L. Gallmann[1] and U. Keller[1*]

Resolving the fundamental carrier dynamics induced in solids by strong electric fields is essential for future applications, ranging from nanoscale transistors[1,2] to high-speed electro-optical switches[3]. How fast and at what rate can electrons be injected into the conduction band of a solid? Here, we investigate the sub-femtosecond response of GaAs induced by resonant intense near-infrared laser pulses using attosecond transient absorption spectroscopy. In particular, we unravel the distinct role of intra- versus interband transitions. Surprisingly, we found that despite the resonant driving laser, the optical response during the light–matter interaction is dominated by intraband motion. Furthermore, we observed that the coupling between the two mechanisms results in a significant enhancement of the carrier injection from the valence into the conduction band. This is especially unexpected as the intraband mechanism itself can accelerate carriers only within the same band. This physical phenomenon could be used to control ultrafast carrier excitation and boost injection rates in electronic switches in the petahertz regime.

Shrinking structure sizes in integrated circuits inevitably lead to increasing field strengths in the involved semiconductor materials[1,2]. At the same time, ultrafast optical technologies enable the extension of operation frequencies of electro-optical devices to the petahertz regime[3]. Both applications ultimately require a deep fundamental understanding of ultrafast electron dynamics in solids in the presence of strong fields for the development of the next generation of compact and fast electronic devices. A number of pioneering experiments demonstrated the potential to measure and control carrier dynamics induced by intense near-infrared laser pulses (peak intensity $I_{peak} \sim 10^{12}\,W\,cm^{-2}$) in semiconductors[4–8] and dielectrics[9,10] on a sub- to few-femtosecond timescale using transient absorption and polarization spectroscopy. So far, resolving such dynamics with attosecond resolution has been limited to the non-resonant excitation regime, where the bandgap of the investigated material is larger than the energy of a single pump photon. Here, in contrast, we unravel the sub-femtosecond response of gallium arsenide (GaAs), a prototype and technologically relevant direct-bandgap semiconductor, in the resonant regime.

Besides the 'vertical' optical transition in the momentum space that corresponds to the absorption of infrared pump photons (so-called interband transition, Fig. 1b), the pump field can also accelerate electrons within the electronic bands (intraband motion, Fig. 1c). In a simplified picture, one can think of inter- and intraband transitions as a consequence of the dual nature of the pump light that behaves either as photons (interband) or as a classical electromagnetic field (intraband). The role of intra- versus interband transitions in the presence of strong electric fields is highly debated[11–17]. For the infrared intensities used in this experiment, we can neglect contributions from the magnetic laser fields[18].

In a recent publication, we demonstrated that during the interaction of a wide-bandgap dielectric such as diamond with a short, intense, non-resonant infrared pump pulse, intraband motion completely dominates the transient optical response[10]. However, it is still unclear whether and how this situation changes in the technologically much more relevant resonant case where a single photon from the pulse has enough energy to induce an interband transition that creates real carriers in the conduction band (CB). The question of whether intraband motion still dominates the interaction and how the coupling between the two mechanisms influences the carrier injection is not obvious and has not been experimentally investigated so far.

To study the electronic response of GaAs when driven out of equilibrium, we combine a 5–6 fs infrared pump pulse (centre energy $\hbar\omega_{IR} \approx 1.59$ eV) with a delayed phase-locked single attosecond pulse (SAP) probe as illustrated in Fig. 1a (further details are given in the Supplementary Information and in ref. [19]). The infrared pump pulse has a peak intensity in vacuum of $\sim 2.31 \pm 0.17 \times 10^{12}\,W\,cm^{-2}$, which corresponds to a peak electric field of $\sim 0.42\,V\,Å^{-1}$. The estimated intensity inside the sample reaches up to 60% of the intensity in vacuum. The two beams are focused into a double target that consists of a gas jet followed by a 100-nm-thick single-crystalline GaAs membrane. The neon gas target enables the extraction of the temporal shape of both pulses as well as a precise delay calibration via a simultaneously recorded streaking measurement[20,21]. We calibrate the time axis of the streaking trace by taking into account the spatial separation of the two targets[22].

The pump–probe principle of attosecond transient absorption spectroscopy is illustrated in Fig. 1. The infrared pulse can induce both inter- and intraband transitions. The SAP probes the modified charge distribution by exciting electrons from the As-3*d* core levels to available states around the bandgap region. Figure 1d shows the measured static absorption spectrum of the GaAs membrane. It is important to note that the broad extreme-ultraviolet (XUV) spectrum of the SAP simultaneously probes the dynamics in the valence band (VB) and the CB.

Figure 2a displays the absorption modification of GaAs induced by the resonant pump pulse, $\Delta\mathrm{Abs}(E,\tau)$ (for definition, see Supplementary Information). A red (blue) region indicates increased (decreased) absorption. In the following analysis, we concentrate on two different delay regimes: (1) when the pump and probe overlap, and (2) when the probe pulse arrives well after the pump.

[1]Department of Physics, ETH Zurich, Zurich, Switzerland. [2]Max Planck Institute for the Structure and Dynamics of Matter, Hamburg, Germany. [3]Present address: Department of Physics, Politecnico di Milano, Milano, Italy. *e-mail: f.schlaepfer@phys.ethz.ch; keller@phys.ethz.ch

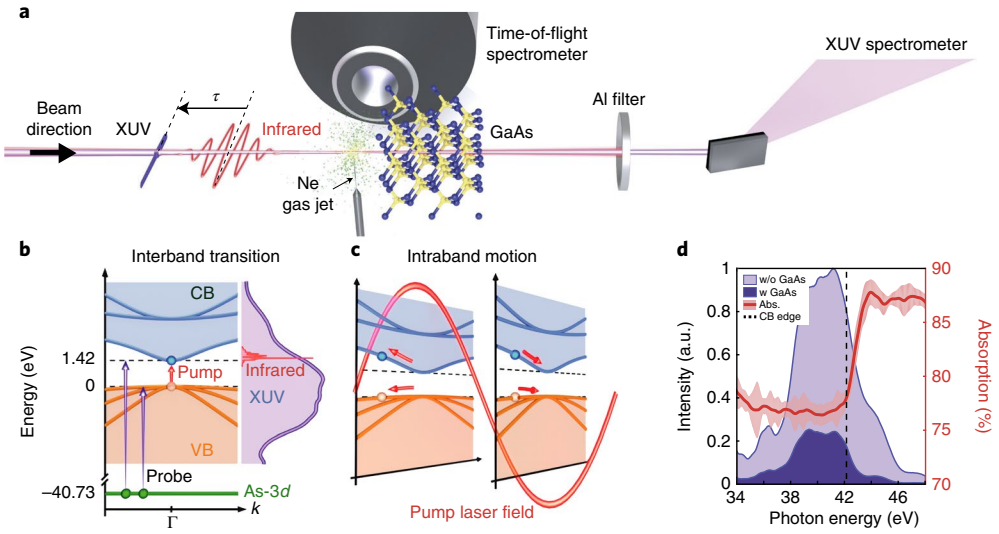

Fig. 1 | Pump–probe mechanism in GaAs. a, Schematic diagram of the experimental set-up with the double-target configuration to perform simultaneous streaking and transient absorption spectroscopy. **b**,**c**, Illustration of the pump-induced dynamics in GaAs. The strong resonant infrared pulse excites carriers either via the absorption of photons from the VB to the CB taking into account nonlinear carrier injection (interband transition, **b**) or accelerates electrons within a band (intraband motion, **c**). The energy axis is defined with respect to the top of the VB. The bandgap of GaAs at room temperature is ~1.42 eV (ref. [29]). The horizontal axis illustrates the crystal momentum k around the Γ symmetry point. The SAP probe measures the distribution of electrons and holes around the bandgap through a transition from the As-3*d* core levels, lying around 40.73 eV below the VB edge[30], to empty states in the VB and CB (violet arrows). In **b**, the spectra for the infrared and XUV pulses are plotted with respect to the top of the VB and the As-3*d* core level, respectively. In **c**, the field-induced carrier motion is illustrated for two instants during the interaction with the infrared pump field. **d**, Transmitted SAP spectrum measured with and without a 100-nm GaAs membrane in the beam path. The red solid line (shaded area) represents the mean value (standard deviation) of the absorption extracted from 42 sets of spectra acquired with and without transmission through the sample.

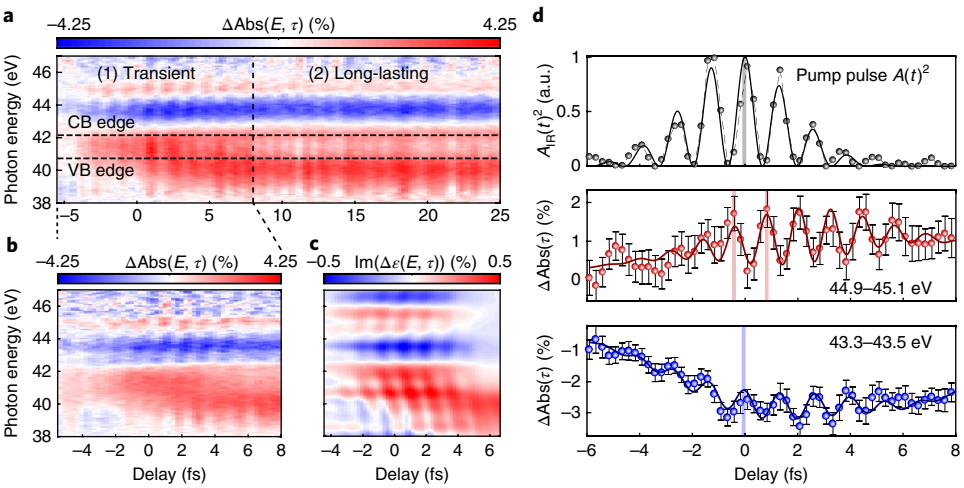

Fig. 2 | Attosecond transient absorption spectroscopy. a, Measured infrared-induced absorption change $\Delta\mathrm{Abs}(E,\tau)$. The interaction is divided into two delay windows: (1) transient response during the pump–probe overlap, and (2) lasting signal after the pump interaction. A positive delay means that the infrared pump comes first and the XUV probe second. We applied a frequency filter to the measured data to reduce the high-frequency noise ($\nu > 1$ PHz). The horizontal black dashed lines mark the position of the VB and CB edge of field-free bulk GaAs. Zero delay is defined by the maximum of the squared vector potential of the pump pulse (see Supplementary Information). **b**, Separate scan over region (1) with longer signal integration, which shows the infrared-induced oscillations in the CB with higher signal fidelity. **c**, First-principles simulation of the imaginary part of the dielectric function, $\Im(\Delta\varepsilon(E,\tau))$, which describes the absorption modification. A positive energy shift of 4.23 eV is applied to the numerical results to correct for the underestimation of the energy gap between the core level and the VB in the first-principles simulation (see Supplementary Information). **d**, Square of the infrared (IR) vector potential extracted from a simultaneous streaking trace and compared with the measured $\Delta\mathrm{Abs}(E,\tau)$ at 43.4 and 45 eV in **b** (0.2 eV integration widths). The dots represent the experimental data, while the solid lines are fits with an oscillatory function to guide the eye. The vertical lines mark the peak position of the fit closest to zero time delay. The phase offset between the two energy windows is also reflected in the tilted shape of the fast oscillating features in **b**. The error bars for the attosecond transient absorption spectroscopy signals include the standard deviation of the mean extracted from 400 signal–reference pairs acquired per delay step and the standard deviation due to the signal variation within the finite-energy integration windows.

Without temporal overlap after the infrared pump pulse, we see a long-lasting signal (that is, regime (2) in Fig. 2a), which persists after the pump interaction over a considerable delay range. During the interaction, electrons are excited via interband transitions from the VB to the CB. This mechanism fully takes into account the nonlinear injection of carriers (see Supplementary Information). The creation of holes in the VB and electrons in the CB causes an increased XUV absorption at the upper VB edge (around 40 eV) and a bleached absorption at the lower CB range (around 43 eV), respectively. The system returns to its equilibrium ground state through electron–hole recombination, which happens for bulk GaAs on a timescale of 2.1 ns (ref. [23]). By looking at negative delays, we can see that the absorption of the system recovers completely between subsequent pulses, which means that there are no accumulative effects and heating of the sample by the laser is negligible.

During the temporal overlap of the infrared pump and the XUV probe pulse, we observe a transient signal (that is, regime (1) in Fig. 2a), which oscillates with $2\omega_{IR}$ and lasts for the duration of the pump pulse (Fig. 2b). The oscillations are visible in a broad probe energy range, most pronounced in the CB between 42.5 and 46 eV. Below 42 eV, they are not well resolved due to stronger fluctuations of the SAP spectral amplitude. However, attosecond transient absorption spectroscopy measurements performed with attosecond pulse trains characterized by a more stable spectrum confirmed the appearance of oscillations also in the VB, around 40 eV (see Supplementary Information).

Figure 2d shows the squared vector potential $A(t)^2$ of the measured infrared pump and the measured transient absorbance for two energy windows. A comparison among them reveals a strong energy dependence of the oscillation phase, which is reflected in the tilted shape of the oscillation features in $\Delta\mathrm{Abs}(E,\tau)$.

To understand the microscopic origin of the measured features, we performed a first-principles electron dynamics simulation (see Supplementary Information for details). We simulated the pump–probe experiment[24] and calculated the pump-induced change of the dielectric function including propagation effects, $\Delta\varepsilon(E,\tau)$, which is directly related to the absorption change $\Delta\mathrm{Abs}(E,\tau)$ (ref. [10]). The numerical results show oscillations with a tilted shape and a long-lasting signal, in good agreement with the experiment (Fig. 2c).

With a decomposition of the probe Hamiltonian of the first-principles simulation into Houston states[10,25], we can disentangle the contributions of the two probe transitions (As-3*d* level to either VB or CB) in the observed dynamics (see Supplementary Information). The energy range above 42 eV, where the strongest transient signal appears, is dominated by probe transitions from the core level to the CB (Fig. 3a). Therefore, in the following, we focus on the CB response.

In a previous study[10], we demonstrated that a non-resonant pump can excite virtual electrons on a sub-femtosecond timescale via intraband motion. Virtual electron excitations live only transiently during the presence of the driving field. For the present experiment, the resonant part of the pump radiation will also inject real carriers into the CB via interband transitions. A population of real carriers persists after the driving pulse has passed and decays orders of magnitude slower than the timescale considered here. To study the ultrafast carriers, we have to investigate the respective signal contributions of infrared-induced intra- and interband transitions. Therefore, we simplify the description of our system to a three-band model, which includes the As-3*d* level, the light-hole VB and the lowest CB (see Supplementary Information). The advantage of the three-band model is that intraband motion and interband transitions between the VB and CB can be numerically included or excluded. Figure 3b shows the CB response with both types of transition involved. The good qualitative agreement with the first-principles decomposition (Fig. 3a) justifies the use of this model to study the respective optical response induced by the two mechanisms.

In the intraband limit, no real electrons are excited from the VB to the CB[26]. This explains why the dielectric function of GaAs fully recovers immediately after the pump pulse (Fig. 3c). In the interband limit, real carriers are injected into the CB by resonant photon absorption, thus resulting in the blue long-lasting signal around 43 eV (Fig. 3d).

In both cases, absorption oscillations with twice the pump frequency appear (Fig. 3e). They originate from the dynamical Franz–Keldysh effect[10,27] (DFKE, intraband limit) and the dynamical Stark effect[28] (interband limit). In contrast to the interband case, the intraband limit clearly shows the strong energy dispersion as in the experiment. In addition, a closer look reveals that the intraband

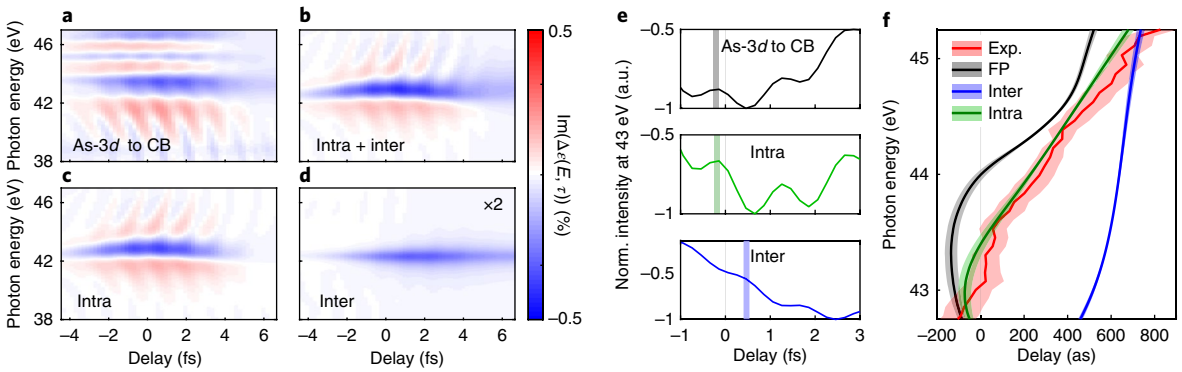

Fig. 3 | Simulated energy- and delay-dependent change of the absorbance. a, Houston decomposition of the first-principles result considering only the As-3*d* to CB probe transition. **b**, Conduction band response in the case of a simplified three-band model. **c**,**d**, The same calculation as in **b** but for the intraband (**c**) and interband (**d**) limit. **e**, Signal at 43 eV (0.2 eV integration width) extracted from **a**, **c** and **d**. **f**, Comparison of the energy-dependent delay between the driving field and the absorption response extracted from the experiment, the first-principles (FP) simulation and the three-band model in the inter- and intraband limit. The experimental delay is the statistical average of nine measurements recorded on four different days. The shaded areas represent the corresponding weighted error bars (see Supplementary Information for details about the extraction method and error definition). The intraband limit calculation is in good agreement with the experiment. The first-principles calculation shows a qualitatively similar trend, however with less good agreement. The residual temporal offset could result from the longitudinal dependence of the infrared intensity in the bulk material (see Supplementary Information). On the other hand, the interband case clearly fails to reproduce the experiment even qualitatively.

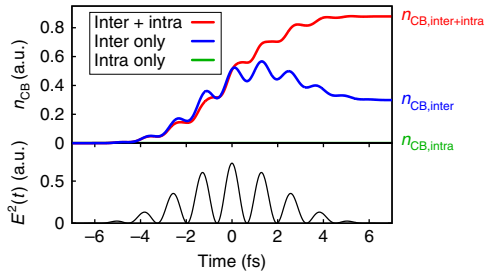

Fig. 4 | Time evolution of the real electron population n_{CB} in the CB extracted from the three-band model. The lower panel displays the square of the instantaneous infrared electric field. Time zero corresponds here to the maximum of the field intensity. In the upper panel, the blue and green curves are the calculated CB populations in the inter- and intraband limit, respectively. Rabi-flopping is responsible for the partial depopulation of the CB during the second part of the pump interaction in the interband limit. Intraband motion does not excite any real carriers into the CB itself. The red curve shows the population with both transition mechanisms involved, intra- and interband. Surprisingly, including intraband motion results in a significantly larger amount of photo-excited carriers compared to the interband limit.

trace oscillates nearly in phase with the decomposed first-principles simulation and therefore with the experimental results, while the inter-band picture clearly fails to reproduce the experimental phase (Fig. 3e).

To further verify this, we compare the energy dispersion of the oscillation delay between the measured and simulated signal for the different models and limits (Fig. 3f). The pure interband case of the three-band model fails to reproduce the experiment while the delay of the intraband limit shows excellent agreement with the experimental results. Therefore, by looking at the attosecond timing of the transient signal, we can conclude that infrared-induced intraband motion (namely the DFKE) dominates the ultrafast response in the CB of GaAs during the pump–probe overlap even in a resonant pumping condition. This is a surprising result, as in the case of a resonant intense pump it is believed that one should not be able to observe DFKE around the bandgap[10,26,27].

Finally, we look at the injection of real carriers from the VB into the CB. We define the CB population, n_{CB}, by the projection of the time-dependent wavefunction of the three-band model on the CB state (see Supplementary Information). In the case of neglected intraband motion (only interband transitions), the calculation predicts a stepwise oscillating increase of n_{CB} following the intensity of the pump pulse (Fig. 4). During the second part of the pump interaction, Rabi-flopping partly depopulates the CB. Surprisingly, in the realistic case involving both excitation mechanisms, the amount of excited carriers increases by nearly a factor of three compared to the model with only interband transitions. This result shows that, although intraband motion does not create real carriers in the CB by itself[26], it assists in the carrier injection initiated by the resonant part of the pump. This indicates that the nonlinear interplay between intra- and interband transitions opens a new excitation channel via virtually excited states at high pump intensities. It is worth emphasizing that the observed enhancement of the injection rate can also be seen in the multi-photon resonant pump regime (see Supplementary Information). Further, it does not depend on the pulse duration. However, using significantly longer pulses or continuous-wave laser light with the same field strength could lead to the target being irreversibly damaged.

To conclude, our measurements and simulations reveal the mechanisms of the sub-femtosecond electron injection in GaAs driven by intense and resonant infrared laser pulses. In contrast to expectations, our results demonstrate that ultrafast transient absorption features, which characterize the early response of the semiconductor to the resonant pump excitation, are dominated by intraband motion, rather than by interband transitions. Furthermore, our simulations show that the virtual carriers created by the intraband motion assist in the injection of real carriers from the VB into the CB. Hence, the interplay between both transition types significantly influences the injection mechanism in the presence of strong electric fields. This process is expected to be universal and persist in a large range of excitation parameters. Therefore, our observation reveals important information about sub-femtosecond electron dynamics in a solid induced by strong fields, which is required for the scaling of the next generation of efficient and fast optical switches and electronics driven in the petahertz regime.

Data availability. The data that support the plots within this paper and other findings of this study are available from the corresponding author upon reasonable request.

Received: 14 August 2017; Accepted: 1 February 2018;
Published online: 12 March 2018

References

1. Mei, X. et al. First demonstration of amplification at 1 THz using 25-nm InP high electron mobility transistor process. *IEEE Electron Device Lett.* **36**, 327–329 (2015).
2. Desai, S. B. et al. MoS_2 transistors with 1-nanometer gate lengths. *Science* **354**, 99–102 (2016).
3. Krausz, F. & Stockman, M. I. Attosecond metrology: from electron capture to future signal processing. *Nat. Photon.* **8**, 205–213 (2014).
4. Schultze, M. et al. Attosecond band-gap dynamics in silicon. *Science* **346**, 1348–1352 (2014).
5. Mashiko, H., Oguri, K., Yamaguchi, T., Suda, A. & Gotoh, H. Petahertz optical drive with wide-bandgap semiconductor. *Nat. Phys.***12**, 741–745 (2016).
6. Sommer, A. et al. Attosecond nonlinear polarization and light–matter energy transfer in solids. *Nature* **534**, 86–90 (2016).
7. Zürch, M. et al. Ultrafast carrier thermalization and trapping in silicon–germanium alloy probed by extreme ultraviolet transient absorption spectroscopy. *Struct. Dyn.* **4**, 044029 (2017).
8. Zürch, M. et al. Direct and simultaneous observation of ultrafast electron and hole dynamics in germanium. *Nat. Commun.* **8**, 15734 (2017).
9. Schultze, M. et al. Controlling dielectrics with the electric field of light. *Nature* **493**, 75–78 (2013).
10. Lucchini, M. et al. Attosecond dynamical Franz–Keldysh effect in polycrystalline diamond. *Science* **353**, 916–919 (2016).
11. Golde, D., Meier, T. & Koch, S. W. High harmonics generated in semiconductor nanostructures by the coupled dynamics of optical inter- and intraband excitations. *Phys. Rev. B* **77**, 075330 (2008).
12. Ghimire, S. et al. Observation of high-order harmonic generation in a bulk crystal. *Nat. Phys.***7**, 138–141 (2011).
13. Malard, L. M., Mak, K. F., Castro Neto, A. H., Peres, N. M. R. & Heinz, T. F. Observation of intra- and inter-band transitions in the transient optical response of graphene. *New J. Phys.* **15**, 015009 (2013).
14. Al-Naib, I., Sipe, J. E. & Dignam, M. M. High harmonic generation in undoped graphene: Interplay of inter- and intraband dynamics. *Phys. Rev. B* **90**, 245423 (2014).
15. Luu, T. T. et al. Extreme ultraviolet high-harmonic spectroscopy of solids. *Nature* **521**, 498–502 (2015).
16. Wismer, M. S., Kruchinin, S. Y., Ciappina, M., Stockman, M. I. & Yakovlev, V. S. Strong-field resonant dynamics in semiconductors. *Phys. Rev. Lett.* **116**, 197401 (2016).
17. Paasch-Colberg, T. et al. Sub-cycle optical control of current in a semiconductor: from the multiphoton to the tunneling regime. *Optica* **3**, 1358 (2016).
18. Ludwig, A. et al. Breakdown of the dipole approximation in strong-field ionization. *Phys. Rev. Lett.* **113**, 243001 (2014).
19. Locher, R. et al. Versatile attosecond beamline in a two-foci configuration for simultaneous time-resolved measurements. *Rev. Sci. Instrum.* **85**, 013113 (2014).
20. Hentschel, M. et al. Attosecond metrology. *Nature* **414**, 509–513 (2001).
21. Itatani, J. et al. Attosecond streak camera. *Phys. Rev. Lett.* **88**, 173903 (2002).
22. Schlaepfer, F. et al. Gouy phase shift for annular beam profiles in attosecond experiments. *Opt. Express* **25**, 3646–3655 (2017).
23. Beard, M. C., Turner, G. M. & Schmuttenmaer, C. A. Transient photoconductivity in GaAs as measured by time-resolved terahertz spectroscopy. *Phys. Rev. B* **62**, 15764–15777 (2000).

24. Sato, S. A., Yabana, K., Shinohara, Y., Otobe, T. & Bertsch, G. F. Numerical pump–probe experiments of laser-excited silicon in nonequilibrium phase. *Phys. Rev. B* **89**, 064304 (2014).
25. Houston, W. V. Acceleration of electrons in a crystal lattice. *Phys. Rev.* **57**, 184–186 (1940).
26. Srivastava, A., Srivastava, R., Wang, J. & Kono, J. Laser-induced above-band-gap transparency in GaAs. *Phys. Rev. Lett.* **93**, 157401 (2004).
27. Novelli, F., Fausti, D., Giusti, F., Parmigiani, F. & Hoffmann, M. Mixed regime of light–matter interaction revealed by phase sensitive measurements of the dynamical Franz–Keldysh effect. *Sci. Rep.* **3**, 1227 (2013).
28. Bakos, J. S. AC stark effect and multiphoton processes in atoms. *Phys. Rep.* **31**, 209–235 (1977).
29. Vurgaftman, I., Meyer, J. R. & Ram-Mohan, L. R. Band parameters for III–V compound semiconductors and their alloys. *J. Appl. Phys.* **89**, 5815–5875 (2001).
30. Kraut, E. A., Grant, R. W., Waldrop, J. R. & Kowalczyk, S. P. Precise determination of the valence-band edge in X-ray photoemission spectra: application to measurement of semiconductor interface potentials. *Phys. Rev. Lett.* **44**, 1620–1623 (1980).

Acknowledgements

We thank M. C. Golling for growing the GaAs, and J. Leuthold and C. Bolognesi for helpful discussion. The authors acknowledge the support of the technology and cleanroom facility at Frontiers in Research: Space and Time (FIRST) of ETH Zurich for advanced micro- and nanotechnology. This work was supported by the National Center of Competence in Research Molecular Ultrafast Science and Technology (NCCR MUST) funded by the Swiss National Science Foundation, and by JSPS KAKENHI grant no. 26-1511.

Author contributions

F.S., M.L., L.G. and U.K. supervised the study. F.S., M.L., M.V., L.K. and N.H. conducted the experiments. M.V. also improved the experimental set-up and data acquisition system. F.S. fabricated the sample and analysed the experimental data. S.A.S. and A.R. developed the theoretical modelling. All authors were involved in the interpretation and contributed to the final manuscript.

Competing interests

The authors declare no competing interests.

Additional information

Supplementary information is available for this paper at https://doi.org/10.1038/s41567-018-0069-0.

Reprints and permissions information is available at www.nature.com/reprints.

Correspondence and requests for materials should be addressed to F.S. or U.K.